PHYSICAL REVIEW E, VOLUME 63, 066209

Characterization, dynamics and stabilization of diffractive domain walls and dark ring cavity solitons in parametric oscillators

Gian-Luca Oppo, Andrew J. Scroggie, and William J. Firth
Department of Physics and Applied Physics, University of Strathclyde, 107 Rottenrow, Glasgow G4 ONG, Scotland, United Kingdom

(Received 5 June 2000; revised manuscript received 16 November 2000; published 17 May 2001)

Mean field models of spatially extended degenerate optical parametric oscillators possess one-dimensional stable domain wall solutions in the presence of diffraction. We characterize these structures as spiral heteroclinic connections and study the spatial frequency of the local oscillations of the signal intensity which distinguish them from diffusion kinks. Close to threshold, at resonance or with positive detunings, the dynamics of two-dimensional diffractive domain walls is ruled by curvature effects with a $t^{1/2}$ growth law, and coalescence of domains is observed. In this regime, we show how to stabilize regular and irregular distributions of two-dimensional domain walls by injection of a helical wave at the pump frequency. Further above threshold the shrinking of domains of one phase embedded in the other is stopped by the interaction of the oscillatory tails of the domain walls, leading to cavity solitons surrounded by a characteristic dark ring. We investigate the nature and stability of these localized states, provide evidence of their solitonic character, show that they correspond to spiral homoclinic orbits and find that their threshold of appearance lowers with increasing pump cavity finesse.

DOI: 10.1103/PhysRevE.63.066209 PACS number(s): 42.65.Pc, 42.50.Lc, 42.82.Fv, 42.50.Gy

I. INTRODUCTION

Mean field (MF) models of degenerate optical parametric oscillators (DOPO) have become the prototype for the study of spatial structures in the presence of quadratic nonlinearities and diffraction. Patterns [1,2], domain walls [3–5], and localized states [4–7] are just a few of the structures recently observed in mean field DOPO. Studies of these structures have been complemented by numerical searches in non-MF models which have confirmed their structural stability [8]. Since MF models allow for analytical studies that are impossible in non-MF equations, we focus here on the characterization of spatial structures in MF equations for the DOPO. Direct experimental evidence of many of these structures in continuous wave (cw) DOPO devices is still lacking but recent developments in the use of large quadratic nonlinearities is promising [9,10], especially for the plane mirror cavities which have been used in theoretical treatments and numerical simulations.

In this paper we focus on the characterization and dynamics of domain walls (DW) separating two homogeneous states of the DOPO. Such DW were first described in MF DOPO models by Trillo, Haelterman, and Sheppard [3] who focused mainly on the one-dimensional transverse case and stabilized a two-dimensional DW structure numerically by means of Neumann boundary conditions. Later we showed that in the two-dimensional case, at resonance and for positive detunings, domains of one homogeneous phase embedded in the other shrink to either zero area or to peculiar localized states characterized by a peak of signal intensity surrounded by a dark ring (the remains of the DW), when close to or far from threshold, respectively [4]. The first aim of this paper is an examination of DW in DOPO at resonance and for positive detunings. Close to resonance, diffractive DW in DOPO differ from diffusive DW as observed, for example, in real Ginzburg–Landau equations, in that spatial local oscillations are present. Such damped oscillations do not appear to affect the behavior of two-dimensional diffractive DW close to threshold where the dynamics of domains of one phase embedded in the other follows the standard $t^{1/2}$ growth law [4]. This is typical of phase separation in systems where the order parameter is not conserved. The second principal aim of this paper is to present a neat arrangement which utilizes a helical pump field to trap and stabilize DW close to threshold along the azimuthal angle of the signal field. Further above threshold the shrinking of domains in the doubly resonant DOPO is stopped by the formation of cavity solitons. The third aim of the paper is to describe some of the properties of these solitons and investigate their existence and stability as a function of the control parameters.

The paper is organized as follows: The behavior of one-dimensional (1D) DW in DOPO is addressed in Sec. II. We point out the possibility of transitions between oscillatory and monotonic behavior in the tails of the DW and present a numerical evaluation of their width. Sec. III is devoted to the two-dimensional dynamics of DW in DOPO close to and away from threshold. The stabilization of DW in the azimuthal direction of a DOPO pumped by a helical wave of topological charge ±1 is discussed in Sec. IV while the dark ring cavity solitons and their stability are analyzed in Sec. V. We also demonstrate by a symmetry argument that DW and dark ring cavity solitons of the degenerate OPO may not survive in the nondegenerate case where the frequencies of the signal and idler fields are substantially different from each other. Section VI contains conclusions and future directions.

II. ONE-DIMENSIONAL DOMAIN WALLS IN MEAN FIELD MODELS OF DOPO

The mean field equations for a phase matched DOPO where both pump and signal fields are resonated [doubly resonant DOPO (DRDOPO), see Fig. 1(a)] are [1]

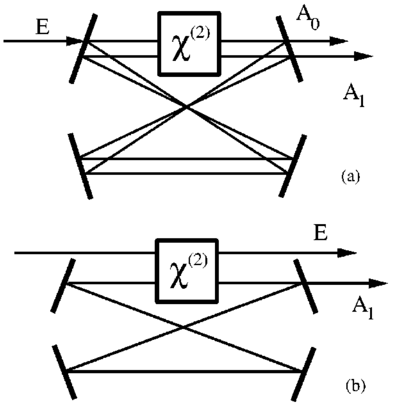

FIG. 1. Schematic of (a) the doubly resonant and (b) the singly resonant degenerate optical parametric oscillator.

$$\partial_t A_0 = \Gamma[-A_0 + E - A_1^2] + \frac{ia}{2}\nabla^2 A_0$$
$$\partial_t A_1 = -A_1 - i\Delta_1 A_1 + A_0 A_1^* + ia\nabla^2 A_1 \qquad (1)$$

where we consider the pump detuning Δ_0 to be always equal to zero unless specified otherwise. For the singly resonant DOPO (SRDOPO) where there is no optical cavity for the pump field [see Fig. 1(b)] the mean field equation for the resonated signal field is [11]

$$\partial_t A_1 = -A_1 - i\Delta_1 A_1 + E A_1^* - A_1|A_1|^2 + ia\nabla^2 A_1. \qquad (2)$$

The slowly varying amplitudes of the pump and signal fields are denoted by A_0 and A_1, respectively, the time has been normalized by the photon lifetime in the signal cavity, $\Gamma = \gamma_0/\gamma_1$ is the ratio between the pump and signal cavity decay rates, E is the amplitude of the external pump field (here assumed to be real), Δ_1 is the signal detuning, and $a = c/\gamma_1 k_z$ is the diffraction parameter with c the speed of light and k_z the longitudinal wave vector of the pump field. Since in the following we will change the ratio between the cavity decay rates, we write the equations without the usual normalizations of the diffraction coefficients with γ_0 and γ_1 [1]. The Laplacian $\nabla^2 = \partial_{xx} + \partial_{yy}$ reduces to ∂_{xx} in one transverse dimension (1D).

A. Spatial equations for DOPO steady states and oscillatory tails

In 1D all steady states (stable and unstable) have to satisfy ordinary differential equations containing spatial derivatives. For the DRDOPO the equations are

$$\partial_{xx} A_0 = \left(\frac{2i\Gamma}{a}\right)(-A_0 + E - A_1^2),$$
$$\partial_{xx} A_1 = \left(\frac{i}{a}\right)(-A_1 - i\Delta_1 A_1 + A_0 A_1^*) \qquad (3)$$

while for the SRDOPO the equation is

$$\partial_{xx} A_1 = \left(\frac{i}{a}\right)(-A_1 - i\Delta_1 A_1 + E A_1^* - A_1|A_1|^2). \qquad (4)$$

Below the threshold for signal generation ($E < \sqrt{1+\Delta_1^2}$) the homogeneous solution $A_0 = E$ and $A_1 = 0$ is stable. Above this threshold and for positive and zero detunings the DOPO equations admit two additional steady state homogeneous solutions given by [3]

$$A_0^s = E - (A_1^s)^2,$$
$$A_1^s = \pm\left(\frac{E I_s}{1 + I_s + i\Delta_1}\right)^{1/2} \equiv \pm\sigma e^{(i\theta)}, \qquad (5)$$
$$I_s = |A_1^s|^2 = \sigma^2 = \sqrt{E^2 - \Delta_1^2} - 1,$$

where $\sigma > 0$ and θ are, respectively, the modulus and phase of A_1^s and

$$\sin(\beta - 2\theta) = \left(\frac{\sigma^2}{2E}\right)\sin\beta, \quad \beta = \arg(1 - i\Delta_1). \qquad (6)$$

In the phase space of Eqs. (3) and (4) the homogeneous states correspond to two fixed points. For the cases of interest here, Trillo, Haelterman, and Sheppard [3] found numerically that a DW solution connecting the two homogeneous states (5) is stable in 1D. They also showed that in the limit of large pump detunings (here set to zero), Eq. (2) reduces to modified nonlinear Schrödinger equation and the DW solution to the standard hyperbolic tangent profile [3]. Such solutions correspond to heteroclinic connections between the two fixed points in the phase space of the fields and their spatial derivatives. We show examples of projections of these heteroclinic connections in Fig. 2 for both doubly and singly resonant cases. Note that in the singly resonant case, where pump diffraction is neglected, the DW oscillations are much smaller. Solutions of the steady state equations (3) and (4) can be found numerically with any required accuracy and can be tested for long term stability via the algorithms specified in the Appendix. We stress here that the presence of heteroclinic and homoclinic solutions in the DOPO is nontrivial. In fact, if we compare Eqs. (4) for $\Delta_1 = 0$ with their diffusive counterpart

$$\partial_{xx} A_1 = \left(\frac{1}{a}\right)(A_1 - E A_1^* + A_1|A_1|^2) \qquad (7)$$

studied, for example, in Ref. [12], we note that the real and imaginary parts of A_1 cannot be trivially decoupled, as they can in (7). Setting the imaginary part of A_1 equal to zero in the diffusive case reduces (7) to an equation governed by a simple quartic potential which admits well-known heteroclinic solutions. Such a simple decoupling, however, is not possible in the diffractive (DOPO) case and the heteroclinic orbits of (3) and (4) cannot be associated with the presence of a quartic potential in any simple limit of these equations.

We note that when $\Delta_1 = 0$, the two stationary solutions A_1^s are purely real and the DW which connects them manifests itself primarily in the real part, R, of the field A_1. In contrast,

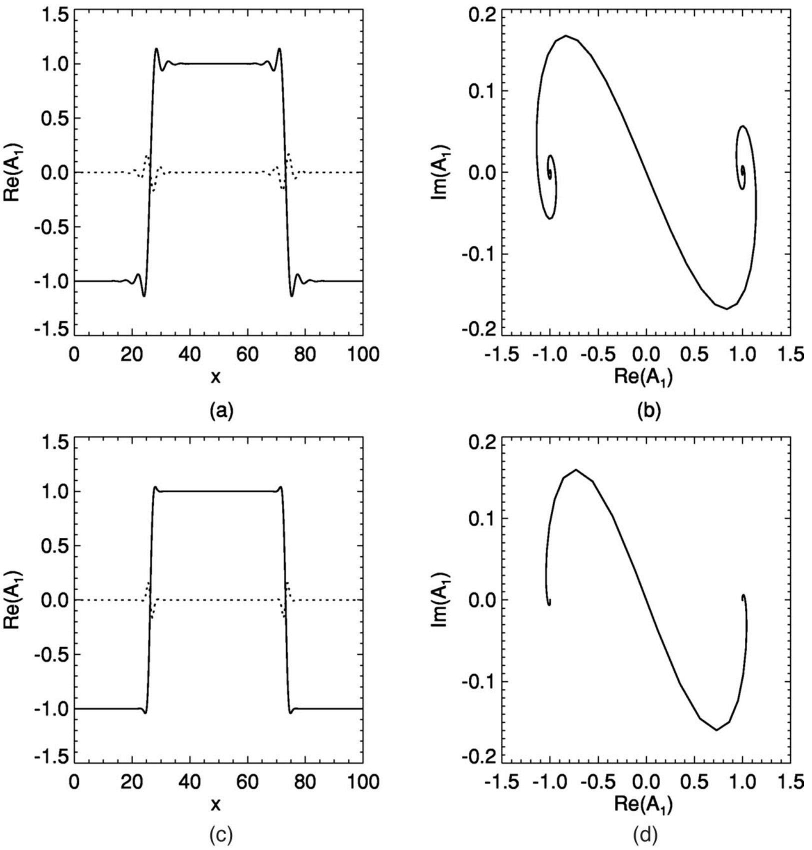

FIG. 2. A heteroclinic solution consisting of a pair of domain walls for $\Delta_1=0.0$, $a=0.5$, $E=2.0$, and $\Gamma=1.0$. (a) Real part (solid line) and imaginary part (dotted line) of the signal field as a function of the transverse coordinate x in the DRDOPO. (b) The DW pair in (a) plotted in the complex A_1 plane. (c) Real part (solid line) and imaginary part (dotted line) of the signal field as a function of the transverse coordinate x in the SRDOPO. (d) The DW pair in (c) plotted in the complex A_1 plane.

the imaginary part, S, of A_1 is zero except in the sharp transition region between the two homogeneous solutions (Fig. 2). When $\Delta_1\neq 0$ the phase, θ, of A_1^s is nonzero and the DW is now observed in the component of A_1 which has the same phase as the two A_1^s. Thus, if we write

$$A_1=R+iS=(U+iV)e^{i\theta} \tag{8}$$

with U and V real, then the field U shows the DW while V is essentially zero. The fields U and V reduce to R and S, respectively, when Δ_1, and hence θ, is zero. The fact that both components of the signal field are zero at the center of these DW indicates that they are Ising walls [12].

The idea that an unstable solution lies at the core of a defect [13] can also be used to explain the fact that $A_1=0$ at the center of the DW. To illustrate this, consider Eqs. (1) for the DRDOPO, without diffraction and with $\Delta_1=0$. Above threshold, the resulting four-dimensional dynamical system has three fixed-point solutions, corresponding to the three homogeneous solutions of Eqs. (1): P_1 with $\mathrm{Re}(A_1)>0$, P_2 with $\mathrm{Re}(A_1)<0$ and O with $\mathrm{Re}(A_1)=0$. The stable manifold of O is the surface $\mathrm{Re}(A_1)=0$. The stable manifolds of P_1 and P_2 are the half-spaces $\mathrm{Re}(A_1)>0$ and $\mathrm{Re}(A_1)<0$, respectively. A continuous function of x representing an initial condition of (1) is mapped onto a one-dimensional manifold in the four-dimensional phase space. A 1D manifold lying entirely in the half-space $\mathrm{Re}(A_1)>0$ $[\mathrm{Re}(A_1)<0]$ evolves towards the solution P_1 (P_2). A 1D manifold which crosses from one half-space to the other intersects the stable manifold of O in a point which moves towards O under the time evolution. This point, where $A_1\to 0$ as $t\to\infty$, corresponds to the center, or ''core,'' of the DW defect. We note, however, that in the DRDOPO case the pump field A_0 is different from E (its stationary value below threshold) at the center of the DW. Such an effect is due to the presence of the pump diffraction.

A DW approaches one homogeneous solution asymptotically as $x\to+\infty$ and the other solution as $x\to-\infty$. Let us focus on the DRDOPO and rewrite system (3) as

$$\partial_{xx}\mathbf{V}=\boldsymbol{\mathcal{N}}(\mathbf{V}), \tag{9}$$

where $\mathbf{V}=[A_0,A_0^*,A_1,A_1^*]^T$ and $\boldsymbol{\mathcal{N}}$ is the appropriate vector-valued function of $\mathbf{V}$. We denote the linearization of the operator $\boldsymbol{\mathcal{N}}$ around a homogeneous, fixed point solution by $\mathcal{L}$: that is, $\mathcal{L}$ is the Jacobian of $\mathcal{N}$ evaluated at A_1^s. Then the behavior of the tails of the DW depends on the nature of $\lambda_{j\pm}=\pm\sqrt{\Lambda_j}$ where $\{\Lambda_j\}$ are the eigenvalues of $\mathcal{L}$. Since

$$\mathbf{V}-\mathbf{V}_{\mathrm{homog}}\sim\sum_{\mathrm{Re}\,\lambda_{j\pm}<0}\alpha_{j\pm}\mathbf{W}_{\mathbf{j}\pm}\exp[(\lambda_{j\pm})x],\quad x\to\infty, \tag{10}$$

where the $\{\mathbf{W}_{\mathbf{j}\pm}\}$ are eigenvectors of $\mathcal{L}$, $\{\alpha_{j\pm}\}$ are complex constants and $\mathbf{V}_{\mathrm{homog}}$ is the stationary homogeneous solution, complex $\lambda_{j\pm}$ imply the possibility of oscillations in the tail of the DW; while monotonic behavior requires (although is not guaranteed by) at least one pair of purely real $\lambda_{j\pm}$.

We remarked previously [4] that at resonance ($\Delta_1=0$) the DW have oscillatory tails for every value of the input pump E and in both the DRDOPO and SRDOPO cases. This is due to the fact that the $\lambda_{j\pm}$ are always complex. Here we point out that for any value of $\Delta_1>0$ real eigenvalues can be found and that hyperbolic tangentlike profiles for the DW, with no oscillatory tails, are possible. For simplicity we start with the SRDOPO case. Tedious but straightforward algebra shows that DW have nonoscillatory tails whenever the following inequality holds:

$$\sqrt{1+\Delta_1^2}<E<\tfrac{1}{2}\sqrt{2+5\Delta_1^2+2\sqrt{1+\Delta_1^2}}. \tag{11}$$

In fact, when (11) is satisfied, two eigenvalues Λ_j are purely real, with opposite sign and with magnitude equal to

$$\sqrt{\frac{1}{a}}[\Delta_1 \pm \sqrt{4I_s(1+I_s)-\Delta_1^2}]^{1/2} \tag{12}$$

while the other two are purely imaginary (corresponding to pure rotations in the phase space). The real positive (negative) eigenvalue corresponds to the unstable (stable) direction of the homogeneous fixed points and the heteroclinic trajectory representing the DW does not spiral around the fixed points. Figure 3(a) shows the region of nonoscillatory DW for the SRDOPO model in the (E,Δ_1) parameter space. Above the onset of oscillatory tails for the DW, we can evaluate the ratio Q between the oscillation frequency and the decay (growth) rate of the stable DW tails for different values of E and Δ_1

$$Q=\frac{\sqrt{4I_s(I_s+1)-\Delta_1^2}}{\Delta_1+\sqrt{4I_s(I_s+1)}}. \tag{13}$$

The ratio Q is plotted as a function of E for different values of Δ_1 in Fig. 3(b). Clearly the maximum value for the ratio Q is one and is obtained at resonance for any value of the external pump E or for large values of E off-resonance (positive detunings). Since the existence of the dark-ring cavity solitons discussed in Ref. [4] and below is associated with large amplitude oscillations of the DW tails which in turn can be obtained only for large values of the ratio Q, we can infer that dark-ring cavity solitons of the kind discussed here are unlikely for the SRDOPO model. To conclude with the SRDOPO case, we note that very close to threshold the behavior of the local oscillations is similar to what is observed for a Swift-Hohenberg equation for one real field (see Ref. [2] and Sec. III). Although localized structures have been observed in a Swift–Hohenberg model far from threshold and for negative detunings [2,14], this is far from the regime where such an equation reliably describes the behavior of the SRDOPO with positive detunings.

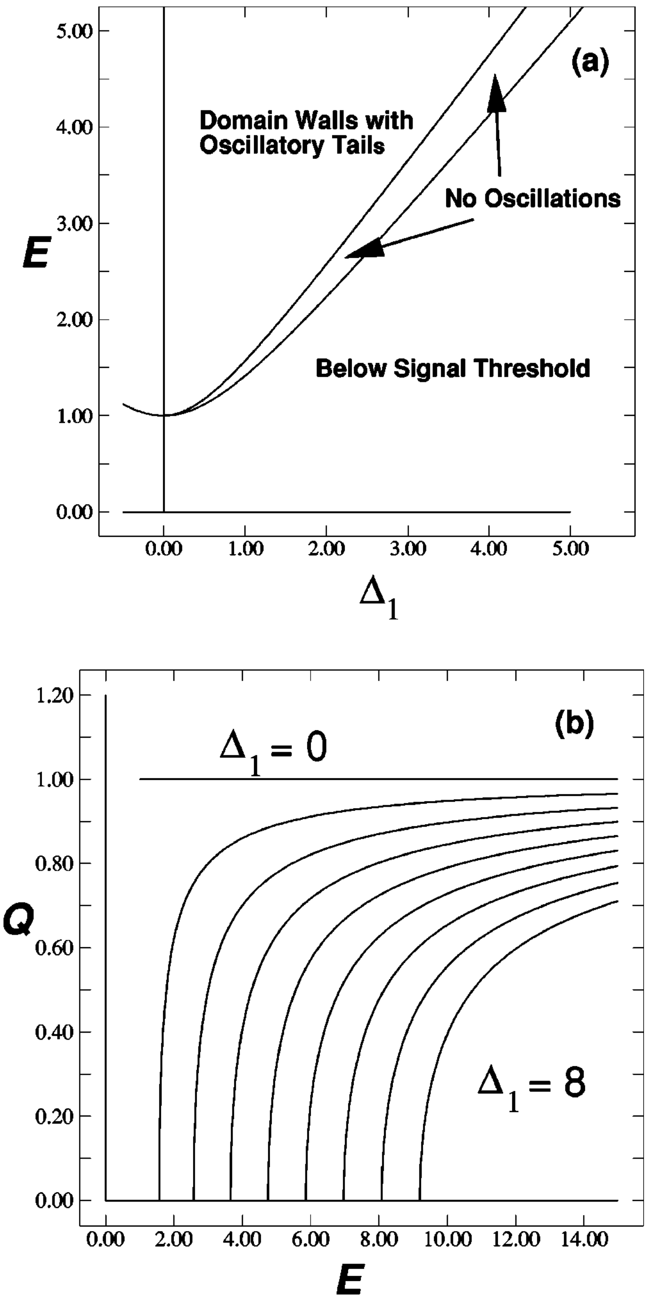

FIG. 3. (a) Parameter region of oscillatory and nonoscillatory tails for the DW in the SRDOPO. (b) The Q ratio between the absolute value of the imaginary and real parts of the complex eigenvalues versus the input pump E. The horizontal curve corresponds to $\Delta_1=0$, the rightmost curve to $\Delta_1=8.0$.

The DRDOPO case does not allow for a picture about oscillatory and nonoscillatory tails of the domain walls as clear cut as the one obtained for the SRDOPO case. This is due to the fact that the spatial stability analysis involves eight eigenvalues Λ_j whose analytical expressions are far too complicated to be reported here. However, by studying their behavior in the (E,Δ_1) parameter space, we can still identify regions where either oscillatory or nonoscillatory DW are to be expected for different values of the time scale ratio Γ. The eight eigenvalues (and eigenvectors) can be separated into two classes; the first (second) class comprises the eigenvalues that do (do not) have a counterpart in the limit of the SRDOPO equation, obtained by letting Γ go to infinity. It is easy to show that the four eigenvalues of the second class (intrinsically due to the presence of a pump equation and pump diffraction) are always complex for any value of E and positive Δ_1. However, close to threshold, the spatial dynamics given by Eqs. (3) is dominated by the first class of eigenvalues where changes from purely real to complex eigenvalues can still take place. We expect nonoscillatory DW in DRDOPO to appear only below the dashed line in Fig. 4(a). This line has been obtained by either locating a transition from purely real to complex eigenvalues (detuning smaller than 1) or a transition from a regime dominated by the first class of eigenvalues to one dominated by the complex eigenvalues of the second class. The latter transition is clearly detectable in the behavior of the eigenvalues by the presence of a cusp point when increasing the pump value E (detunings larger than 1). Unlike the SRDOPO case [see Fig. 3(a)], the separation line between nonoscillatory and oscillatory DW of Fig. 4(a) is now just an estimate and not an exact result since for any value of the parameters (E,Δ_1) of the DRDOPO there is at least one complex eigenvalue. Such an estimate, however, agrees very well with the numerical results and can be used as an excellent guide to the character of the DW in DRDOPO.

Above the dashed line of Fig. 4(a), the second class of complex eigenvalues governs the spatial dynamics of the DW. Figure 4(b) shows the ratio Q between imaginary and real parts of the significant eigenvalue belonging to the second class. We stress here that such a class of eigenvalues has no counterpart in the SRDOPO case since they move progressively away to infinity for larger and larger values of the ratio $\Gamma=\gamma_0/\gamma_1$. In contrast to the SRDOPO case [Fig. 3(b)], Fig. 4(b) shows that spatial oscillations of DW can grow substantially in DRDOPO since the maximum value of Q is not constrained to be equal to 1. It is such large amplitude oscillations close to the boundary of the domain walls that allows for the formation of the dark ring cavity solitons discussed in Sec. V. The interaction of large amplitude oscillating tails of the DW leads to the stabilization of homoclinic orbits with signal intensities much greater than the homogeneous value.

B. Effective width and pairwise interactions

Strictly speaking, the ‘‘width’’ of a domain wall is infinite. We can, however, try to quantify the sharpness of the transition between the two homogeneous solutions in a fairly simple way.

To compute the width of a DW, we calculate the slope of U [Eq. (8)] at the center of the DW $(x=x_c)$, where U is zero. We then extrapolate linearly in each direction, for a distance $\Delta x/2$, until we reach the appropriate homogeneous solution, U^s. The width of the DW is then taken to be

$$\Delta x=2U^s\left[\left.\frac{dU}{dx}\right|_{x=x_c}\right]^{-1}. \tag{14}$$

An alternative definition of the DW width can also be given in terms of the signal amplitude. We calculate the slope of $|A_1|$ at the point where it is zero, which corresponds to the center of the DW, and extrapolate linearly for a distance $\Delta x_{\rm mod}/2$ until the homogeneous solution $|A_1|^s$ is reached. Thus

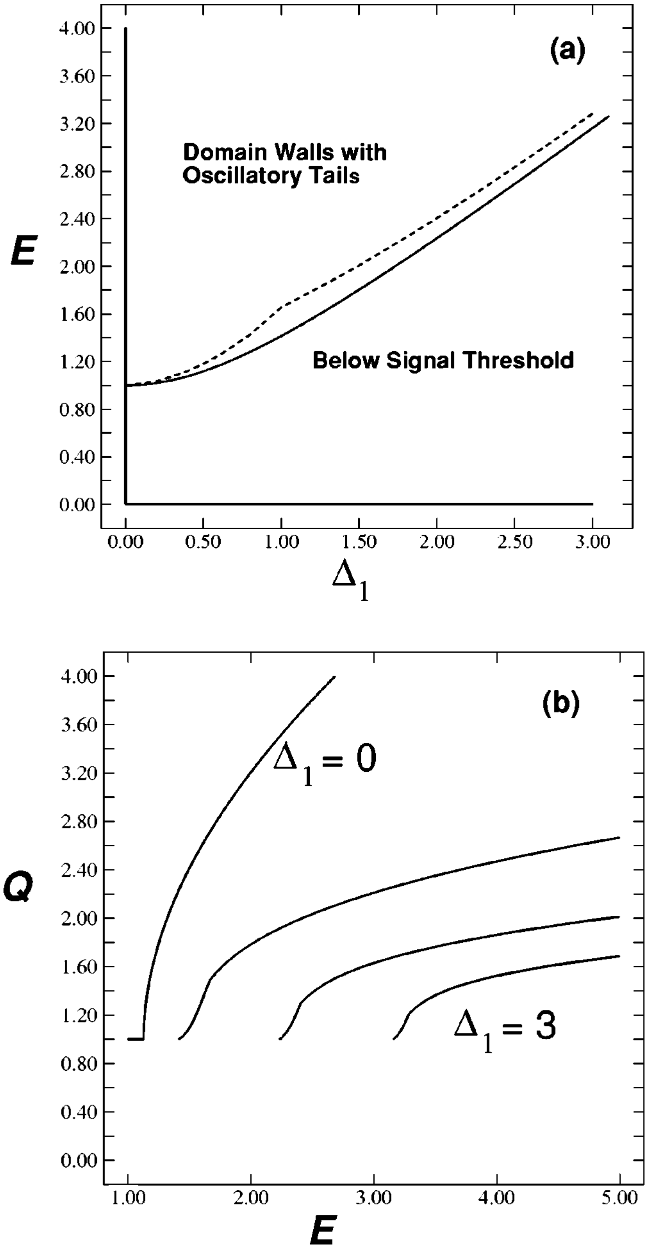

FIG. 4. (a) Approximate separation between parameter regions of oscillatory and nonoscillatory tails for the DW in the DRDOPO for $\Gamma=1$. (b) The Q ratio between the absolute value of the imaginary and real parts of the complex eigenvalues. The leftmost curve corresponds to $\Delta_1=0$, the rightmost curve to $\Delta_1=3.0$.

$$\Delta x_{\rm mod}=2|A_1|^s\left[\left.\frac{d|A_1|}{dx}\right|_{x=x_c}\right]^{-1}. \tag{15}$$

This definition includes the contribution to the DW width of the field V, which can be different from zero in the vicinity of the point where the signal intensity is zero. The difference between the two measures of DW width, however, is found to be on the order of 2% at most. We will therefore use the definition (14).

DW solutions to Eqs. (1) or (2) can be obtained by integrating the partial differential equations directly using a

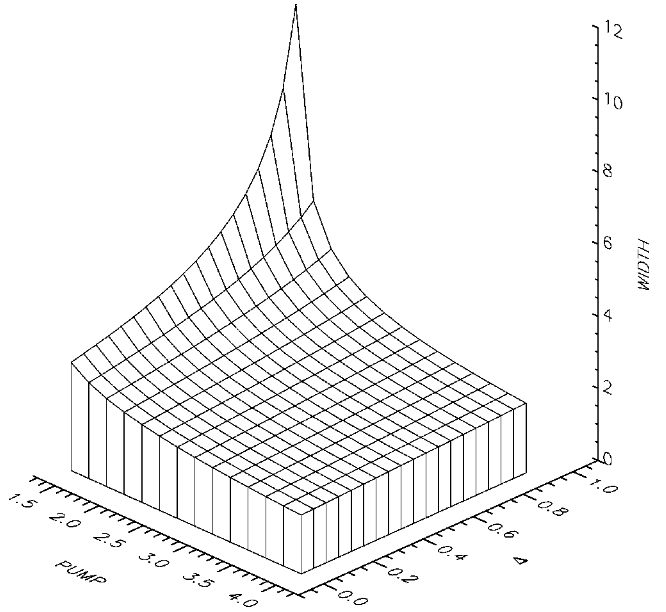

FIG. 5. Width of DW in the DRDOPO as a function of the pump amplitude E and the detuning Δ_1.

split-step spectral method [15], where the diffractive terms are handled by an FFT and the remaining terms by a fourth-order Runge-Kutta technique. Such a method is cumbersome, requires a lot of CPU time and allows for the analysis of stable DW only. Alternatively, the method described in the Appendix which computes stable and unstable stationary solutions of Eqs. (1) or (2) can be used. With either method, the computed solution is the same if the DW solution is stable. The width of the DW can then be evaluated numerically according to Eq. (14).

As an example, Fig. 5 shows how the width of the DW in the DRDOPO varies with the detuning Δ_1 and the external pump E. Moving away from threshold, DW with or without oscillatory tails progressively narrow. Far from threshold, the width of the DW tends to remain almost constant for a wide range of values of the detuning and pump parameters. Since away from resonance DW with nonoscillatory tails appear only close to threshold, DW with oscillatory tails are narrower than DW with monotonic tails for any fixed value of the detuning Δ_1. The effective width of the DW is a useful parameter in the understanding of the interactions of DW.

An adjacent pair of domain walls, if stationary, represents a homoclinic trajectory in the phase space of Eqs. (3) and (4): the fields start close to one homogeneous solution for large negative x and end up back at the same homogeneous solution for large positive x. In diffusive systems, such DW pairs are generally unstable since they exert a mutual, though exponentially decaying, attraction [16,17]. Numerical realizations of such solutions can appear stable since the discretization imposed by the grid can make the small attractive ‘‘force’’ jump to zero for sufficiently large separations. Numerical DW pairs with nonoscillatory tails will however move towards each other and mutually annihilate if they are close enough, in a way similar to what happens in purely diffusive cases.

The behavior of diffractive DW with oscillatory tails is somewhat different. Again, for sufficiently large separations, each DW is essentially independent: the distance between them can be increased or decreased with no apparent constraint. The method described in the Appendix allows for the evaluation of the Jacobian of Eqs. (1) at a stationary solution consisting of a pair of widely separated DW. Such a Jacobian has two zero eigenvalues: one corresponding to an overall translational invariance of the solution, and the other, to a relative motion of the two DW.

The presence of two zero eigenvalues remains true until the DW are close enough for their oscillating tails to interact. When this happens, a locking phenomenon occurs which permits only a discrete set of stationary DW separations. Some examples of the resulting structures together with the largest of the nonzero eigenvalues of the equations linearized about each solution are shown in Figs. 6(a)–6(f). For any initial condition with a given separation of DW with oscillatory tails, the distance between the DW relaxes to the closest of these equilibrium values. No coarsening process is observed. Similar behavior has been noted in other systems [17] where pairs of spatial solitary waves or fronts between homogeneous solutions are known to be stationary at positions where the maxima and minima of their oscillating tails approximately coincide. Demonstrations of the existence of an interaction potential between fronts, however, are only possible in the limit of small amplitude spatial oscillations and long-range interactions and only in systems with a variational structure [17]. Nevertheless, the phenomenon appears to be general even when an explicit potential function is unobtainable.

Compare Fig. 6 with what happens when the DW have no oscillating tails. Guided by the results of the preceding subsection, we have increased Δ_1 in Fig. 7 to the point where the spatial oscillations disappear. The result is that the DW approach each other and annihilate, without any intermediate stationary state [18]. (Note, however, that two DW must be very close to each other in order for their weak interaction to induce motion within any computationally tractable time span. This is compounded by the effect, mentioned previously, whereby the spatial discretization may force the interaction to go to zero.) The ability to observe both kinds of DW behavior by suitably varying one or more parameters is one of the most interesting features of the OPO.

III. DYNAMICS OF DW IN THE TWO-DIMENSIONAL DOPO

In two dimensions, the two possible states of the OPO [Eq. (5)] manifest themselves as domains of one solution embedded in the other, the boundary consisting of a (closed) domain wall. The curvature of the DW causes it to move and the enclosed domain to contract [4,5].

Figures 8 and 9 show typical examples of the evolution of the DRDOPO signal real part and intensity, respectively, close to threshold and for $\Delta_1 = 0$. The simulations in Fig. 8 use periodic boundary conditions while a more realistic finite width input pump of hyperbolic tangent shape is used for Fig. 9. In both of these cases there is a coarsening over time as domains shrink and ultimately disappear: in the long term,

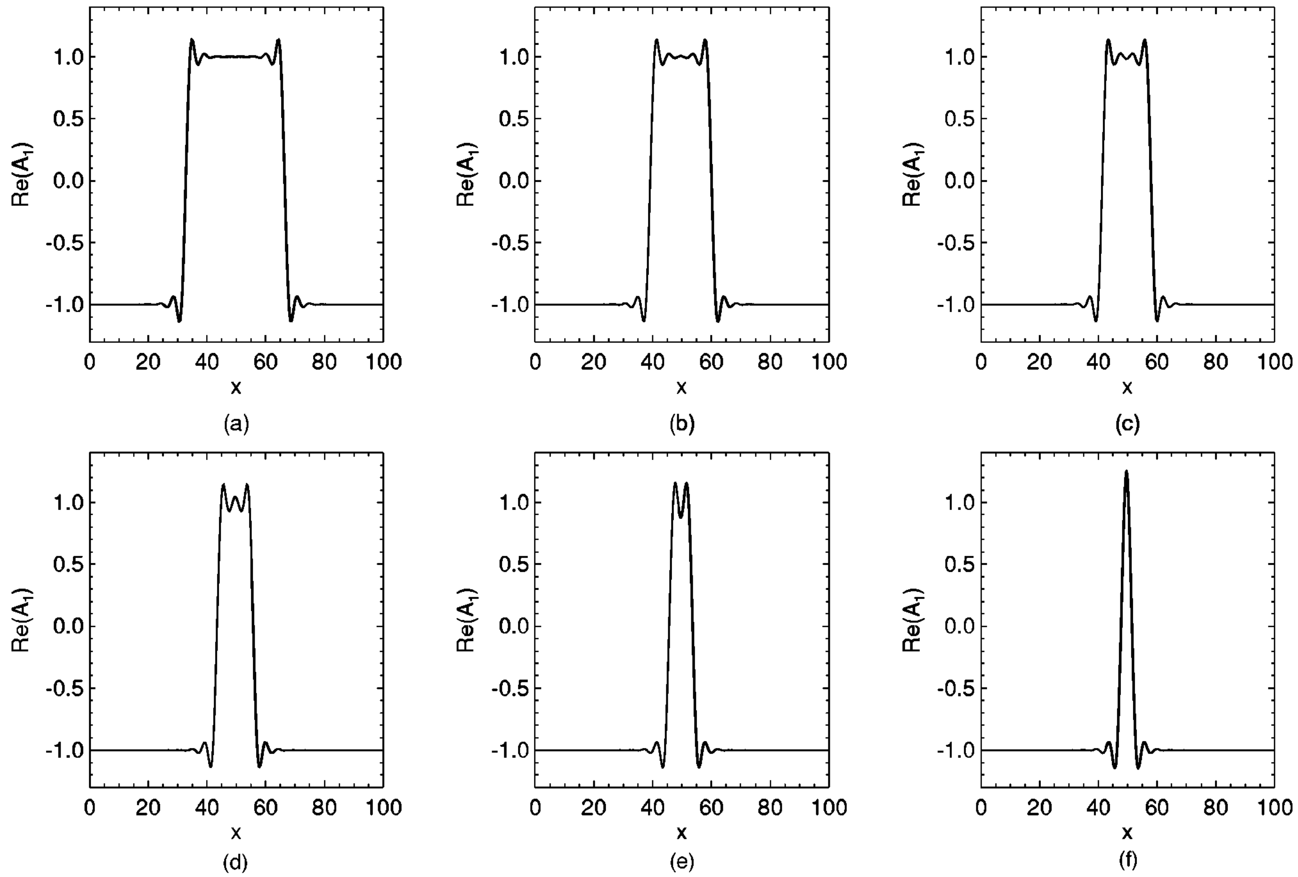

FIG. 6. Stationary DW pairs separated by various distances. All solutions shown are both stationary and stable. Other intermediate stationary solutions exist, both stable and unstable. Parameters as in Fig. 2. The largest nonzero eigenvalues of the equations linearized around these solutions are (a) $-0.000\,000\,3685$, (b) $-0.000\,1319$, (c) $-0.000\,9383$, (d) $-0.006\,748$, (e) -0.0511, (f) -0.4131.

only one of the two homogeneous phases survives. The presence of a finite width pump also causes the DW to curve since they try to be perpendicular to the circular boundary.

The evolution is analogous to phase separation in systems far from equilibrium where the order parameter is not conserved [19]. To test this hypothesis we can define a two-point spatial correlation function $C(r,t)$ as

$$C(r,t)=\frac{\langle A_1(\vec{r}_0+\vec{r},t)A_1(\vec{r}_0,t)\rangle_{\vec{r}_0}}{\langle A_1(\vec{r}_0,t)A_1(\vec{r}_0,t)\rangle_{\vec{r}_0}}, \qquad (16)$$

where the average is over the initial position $\vec{r}_0$ and different realizations, and a structure factor $S(k,t)$ (its Fourier transform) as

$$S(k,t)=\frac{1}{2\pi}\int \exp(ikr)C(r,t)dr. \qquad (17)$$

In systems where the dynamics of random phase domains is dominated by local curvature effects, the characteristic size of domains exhibits a $t^{1/2}$ growth law and the structure factor scales as [19,20]

$$S(k,t)=t^{1/2}f(kt^{1/2}). \qquad (18)$$

Such a scaling can be demonstrated for Ising models and has been verified numerically and experimentally in a variety of systems [19].

Figure 10 shows the structure factor S calculated for a single simulation of the DROPO equations (parameters corresponding to Fig. 8) showing the same scaling behavior. This indicates that the dynamics of domains in the DOPO is the same as that in phase separation with a nonconserved order parameter, at least close to threshold, despite the fact that the underlying physical processes are different. All closed domains are therefore expected to disappear, the asymptotic states being either one of the two homogeneous states or exceptionally, in the case of periodic boundary conditions, an even number of parallel DW. For completeness, Fig. 11 plots correlation functions [Eq. (16)] evaluated at intervals of 30 signal photon cavity lifetimes for the same simulation as in Fig. 10. The inset shows that when these same correlation functions are plotted as functions of $r/t^{1/2}$, they lie on top of each other. This clearly indicates a growth $\sim t^{1/2}$ of the characteristic size of domains. Both Figs. 10 and 11 extend to a time of around 300 signal photon cavity lifetimes for simulations on a 256×256 grid. For longer times the exponent of the growth law may deviate from the value 1/2 due to finite size effects.

Note that in the case of a radially symmetric finite size input pump, the DW tend to be perpendicular to the bound-

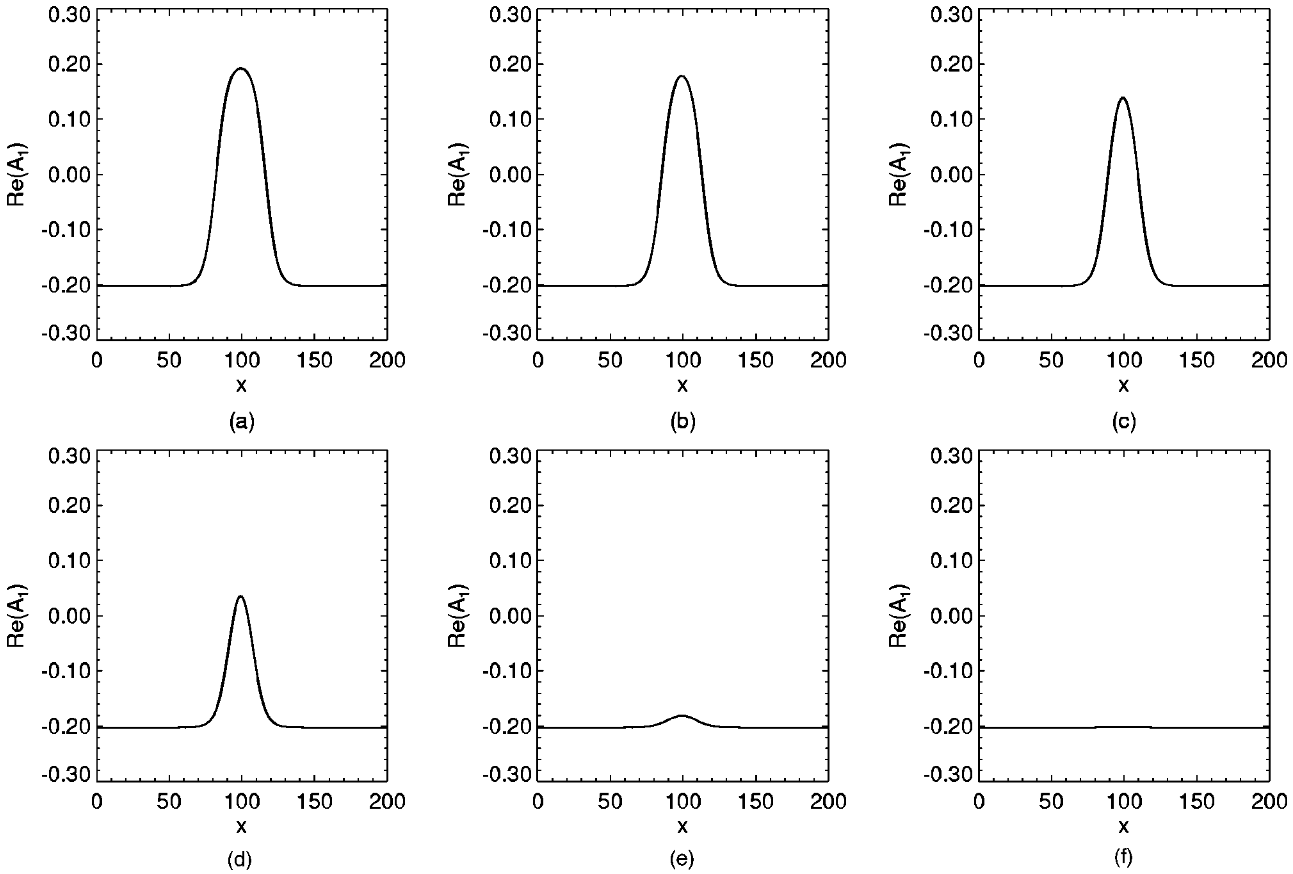

FIG. 7. A pair of nonoscillatory DW approaching each other and collapsing. To avoid a prohibitively long transient, the walls are initially placed quite close to each other. (a) $t=0$, (b) $t=2400$, (c) $t=2800$, (d) $t=2880$, (e) $t=2960$, and (f) $=3040$. $\Delta_1=1.7$. All other parameters as in Fig. 2.

ary, introducing a further local curvature for straight DW which do not cross the center of the pump beam. This effect further limits the number of asymptotic states obtainable in a realistic DOPO. For generic initial conditions we expect all DW to disappear after transients. For this reason we have devised a clever arrangement for an asymptotic stabilization of DW making use of helical pump waves as described in the next section.

It is not obvious why the DOPO should show the same scaling behavior as systems undergoing phase separation. No free energy functional exists for the former, nor is there any direct, explicit analog of surface tension. (In addition, after our report of this phenomenon [4], further evidence of such scaling has appeared in other nonlinear optical systems with no free energy functional [21].) In the DOPO, close to threshold and for Δ_1 small and positive or zero, the dynamics can be approximately described by a real Swift–Hohenberg (SH) equation [2] of the form

$$\partial_t F=\frac{(E-E_0^{\mathrm{SH}})}{E_0^{\mathrm{SH}}}F-\frac{F^3}{(1+\Delta_0^2)}-\frac{1}{2}(\Delta_1-a\nabla^2)^2F, \tag{19}$$

where $E_0^{\mathrm{SH}}=(1+\Delta_0^2)^{1/2}$ and

$$F=A_1e^{-i\psi},\quad e^{2i\psi}=\frac{E_0^{\mathrm{SH}}}{(1+i\Delta_0)}. \tag{20}$$

The SH equation *is* variational and its free energy has a surface tensionlike contribution which favors the minimization of domain boundaries. Moreover, it has been shown [14] that the dynamics of domains in the SH equation is governed by the same local curvature effects as is that of phase separation [22]. For Δ_1 positive and $O(1)$, the normal form equation is, instead, of Ginzburg-Landau (GL) type [2]:

$$\partial_t F=\frac{(E-E_0^{\mathrm{GL}})}{E_0^{\mathrm{GL}}}(1+\Delta_1)^2F-\frac{(1-\Delta_0\Delta_1)}{(1+\Delta_0^2)}F^3+a\Delta_1\nabla^2F, \tag{21}$$

where $E_0^{\mathrm{GL}}=(1+\Delta_0^2)^{1/2}(1+\Delta_1^2)^{1/2}$ and

$$F=A_1e^{-i\psi},\quad e^{2i\psi}=\frac{E_0^{\mathrm{GL}}}{(1+i\Delta_0)(1+i\Delta_1)}. \tag{22}$$

The Ginzburg–Landau equation, again, has a free energy, surface tension, and dynamics driven by local curvature [19].

This is not the whole story, however. The normal form equation, whether Swift–Hohenberg or Ginzburg-Landau, is only valid near threshold. Even quite far from threshold

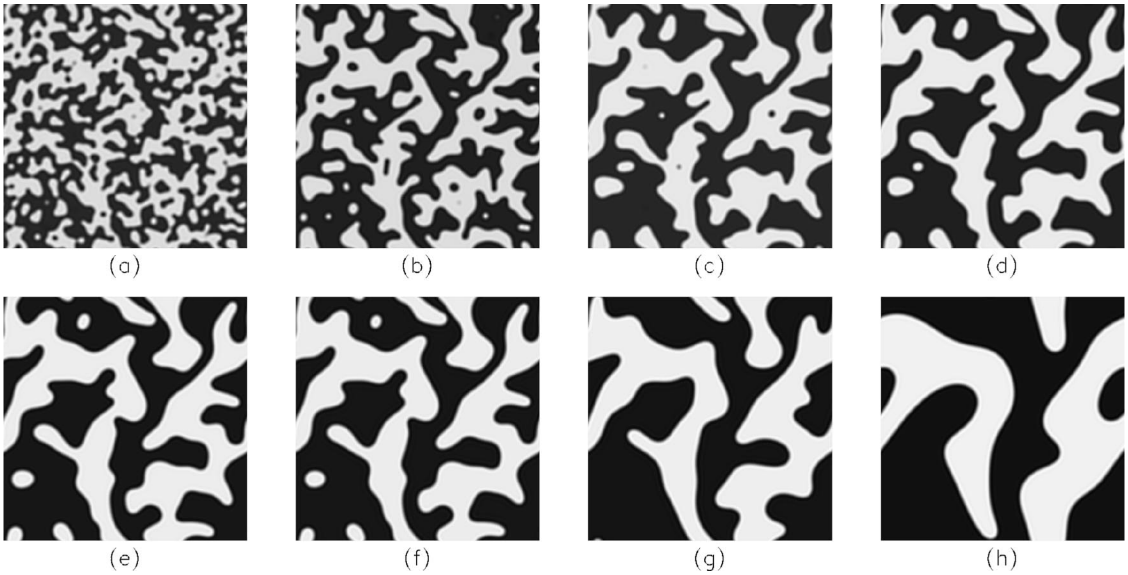

FIG. 8. Phase dynamics in the DRDOPO. The figures show Re(A_1) in the transverse plane at (a) $t=30$, (b) $t=90$, (c) $t=150$, (d) $t=210$, (e) $t=270$, (f) $t=300$, (g) $t=540$, and (h) $t=1500$. $E=1.4$, transverse domain width 250 and other parameters as in Fig. 2.

where the SH or GL equation no longer applies, the system still tries to minimize the surface ''area'' of domain boundaries by causing domains to shrink. Although it is impossible to attribute a variational structure to the OPO equations [23] or to identify a term which plays the role of a surface tension, the phase-separation behavior with a $t^{1/2}$ growth law persists and is therefore seen to occur in a larger class of systems than merely those which possess a free energy.

If the pump amplitude E is large enough in the DRDOPO, then the collapse of shrinking domains is arrested by the formation of solitary-wave-type structures (Fig. 14). This phenomenon is not observed in the SRDOPO, where domains continue to shrink to zero area no matter how large the amplitude of the pump. The DRDOPO ''cavity solitons'' will be discussed further in Sec. V.

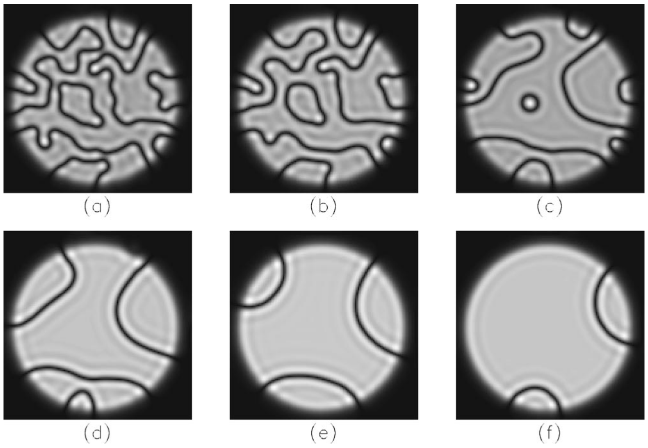

FIG. 9. Phase dynamics in the DRDOPO pumped by a finite size beam. The figures show the intensity of the signal field in the transverse plane at (a) $t=10$, (b) $t=20$, (c) $t=80$, (d) $t=150$, (e) $t=350$, (f) $t=600$. Transverse domain width 20π and other parameters as in Fig. 2.

Before ending this section we remark on the relevance, or otherwise, of domain dynamics, growth laws and scaling behavior to the one-dimensional case. In 1D there is no analog of DW curvature and the motion of a DW is driven only by its interaction with other DW. As stated in Sec. II, these interactions fall off so rapidly with distance that DW dynamics are essentially unobservable in 1D for times that are computationally accessible. Even in the case where the domain size is made so small that DW with nonoscillatory tails are forced to interact, we have been unable to discern any growth law or scaling behavior of the structure factor.

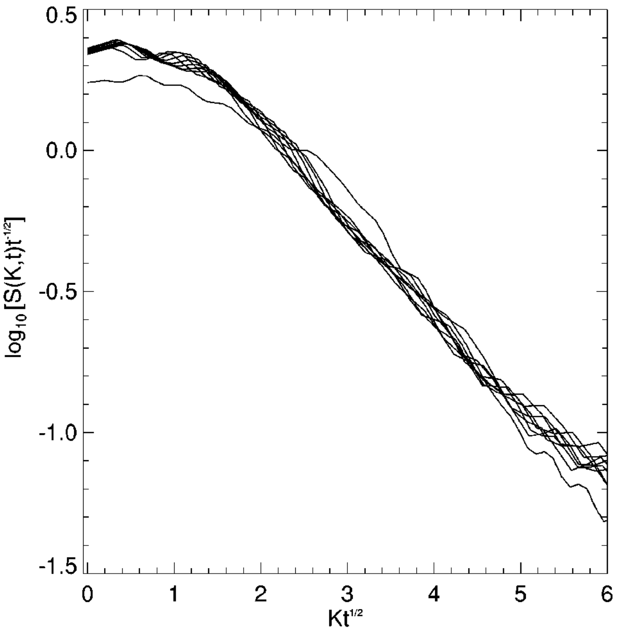

FIG. 10. Plot of $\log_{10}(S/\sqrt{t})$ as a function of $K\sqrt{t}$ at time intervals of 30 signal photon lifetimes from $t=30$ to $t=300$. Parameters as in Fig. 8.

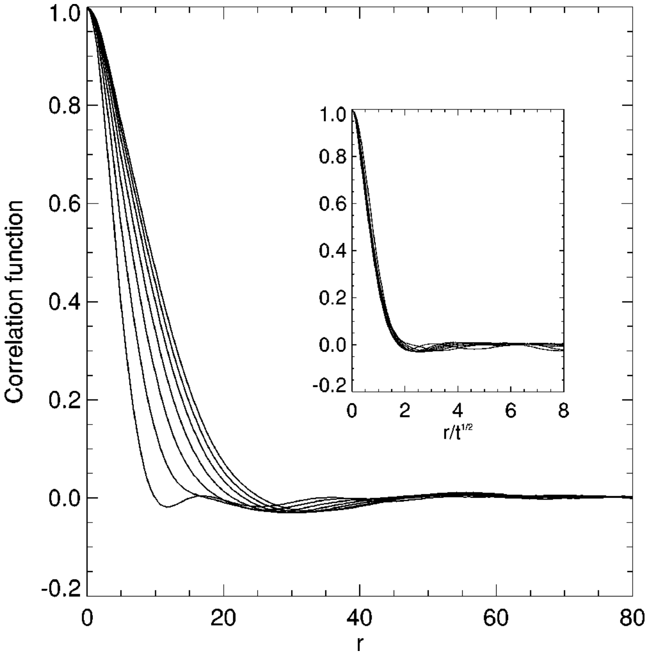

FIG. 11. Plots of the correlation function evaluated at intervals of 30 signal photon lifetimes for the same simulation as in Fig. 10. The inset plots the same correlation functions against $r/t^{1/2}$.

IV. STABILIZATION OF DW IN A DOPO PUMPED BY HELICAL WAVES

In the preceding section we have seen that in two transverse dimensions DW appear only during transients. When walk-off is present, trains of DW quickly move across and out of the optical beam [24]. In the next section we will show that the dark rings surrounding cavity solitons are not circular DW since they remain very far from one of the homogeneous solutions. These features seem to suggest that an experimental observation of stable DW in cw DOPO can be elusive. It is the aim of this section to illustrate simple experimental configurations where DW are asymptotically trapped, thus allowing one to study and characterize these intriguing spatial structures in real OPO devices.

We introduce into the configurations of Fig. 1 an external pump with a single Gauss-Laguerre (GL) mode profile,

$$E(x,y)=E_0(2\rho^2)^{|m|/2}L_p^m(2\rho^2)e^{-\rho^2+im\phi}, \tag{23}$$

where E_0 is the (real) amplitude of the GL mode, ρ and ϕ are the polar coordinates spanning the transverse plane, p and m are the radial and angular indices of the GL mode, and L_p^m is the GL polynomial of the given argument [25]. The GL modes with $m=0$ have large intensities at the center of the beam while as soon as $m\neq 0$ the intensity at the origin of the transverse plane vanishes. Propagating GL modes with $p=0$ and $m\neq 0$ are also commonly referred to as helical waves, the direction of the twist being related to the sign of the index m. It is exactly on the utilization of input helical waves at the pump frequency that our method of stabilization of DW is based.

In this paper we focus on the stabilization of DW at resonance, i.e. $\Delta_1=0$, since many of the features of the procedure can easily be generalized to the detuned case. First we look for stationary solutions in the presence of input helical waves. By writing the input, pump and signal fields as

$$E(x,y)=Q(r)e^{im\phi}, \quad A_0=C_0(r)e^{im\phi}, \quad A_1=C_1(r)e^{im\phi/2} \tag{24}$$

we obtain steady state equations for the radial functions $C_0(r)$ and $C_1(r)$ given by

$$ia\nabla_r^2C_0(r)-\left(2+\frac{iam^2}{r^2}\right)C_0(r)+2Q(r)-2C_1^2(r)=0,$$

$$ia\nabla_r^2C_1(r)-\left(1+i\Delta_1+\frac{iam^2}{4r^2}\right)C_1(r)+C_0(r)C_1^*(r)=0, \tag{25}$$

where

$$\nabla_r^2\equiv\frac{1}{r}\frac{\partial}{\partial r}\left(r\frac{\partial}{\partial r}\right). \tag{26}$$

These conditions have to be completed with the requirement of continuity (modulo 2π) of the signal phase over rotations of integer multiples of 2π. It is clear from (24) that continuity of the phase can only be achieved with m even and indeed we find purely radial stationary states $C_0(r)$ and $C_1(r)$ only in such cases. In the case of m odd, there is an accumulated phase of π which remains trapped within the output structure and no stationary states exist. This accumulated phase is ''discharged'' by a DW in the radial direction. Such a DW is localized in ϕ, the azimuthal coordinate, in the same way that its Cartesian analog is localized in x.

Figure 12 shows asymptotic spatial signal amplitudes for different values of the input topological charge m and various initial conditions. In the case of m equal to an odd integer, the total number of DW trapped in the beam is always an odd number while for m even, zero or an even number of DW are observed in the signal output. The presence of trapped domain walls in the case of $m=2$ [see Fig. 12(f)] does not contradict our previous considerations. The phase can jump several times by $\pm\pi$ during a loop of the central spot but the total number of jumps has to be odd for m odd and even for m even in order to satisfy (24).

Whenever the asymptotic solution contains a number of trapped DW, the signal intensity rotates around the optical axis at a constant speed. The frequency of rotation depends on the topological input charge m but not on the number of trapped DW. So, for example, the speed of rotation is the same for the configurations displayed in Figs. 12(a)–12(d) since $m=1$. The rotation of the DW is always in the direction of growing pump phase as expected for spatially localized structures [26].

In order to find an analytical expression for the angular frequency of the rotations, we consider an input field of the form given by (24) and the following ansatz for the pump and signal fields

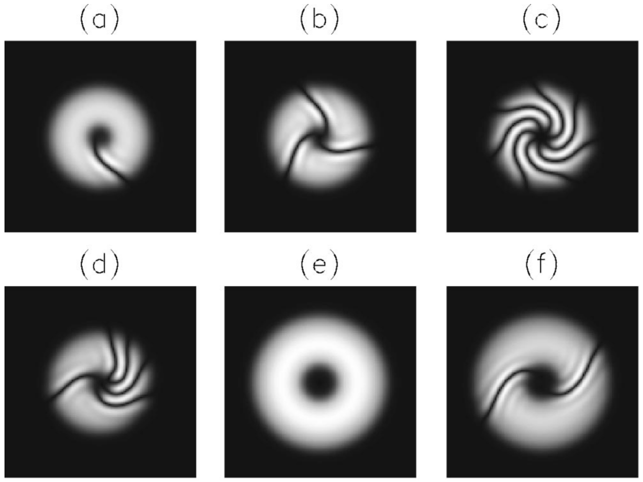

FIG. 12. Stable output configuration of the signal intensity for a DRDOPO pumped by a Gauss–Laguerre mode of azimuthal index $m=1$ [panels (a)–(d)] and $m=2$ [panels (e) and (f)]. Transverse domain width 20π, $E=2.0$ for panels (a)–(d), $E=3.0$ for panels (e) and (f) and other parameters as in Fig. 2.

$$A_0=C_0(r)g_0(r,\phi-\omega t)e^{im\phi},$$
$$A_1=C_1(r)g_1(r,\phi-\omega t)e^{im\phi/2}. \tag{27}$$

Solutions of this form rotate with a fixed frequency ω. Substituting the ansatz (27) into Eqs. (1) and comparing with (25), one is left with

$$\omega=a\frac{m}{r^2}. \tag{28}$$

This expression suggests a motion of the trapped domain wall in the direction of increasing phase of the input pump in agreement with Ref. [26], a zero rotation in the absence of diffraction, and a radially dependent angular velocity. The latter feature would, in principle, progressively shear the DW during its temporal evolution. Such a shear mechanism is however counterbalanced by the curvature effect of two-dimensional DW that favors straight DW as described in the preceding section. Indeed, close to threshold we observe in the numerical simulations almost straight, radially directed DW trapped in the signal beam, in good agreement with the previous argument. Away from threshold, the shear effect of (28) is visible in the local curvature of the trapped domain wall. The curvature effect requires a straightforward modification of the expression for the frequency of rotation to include radial averages. This is easily achieved by replacing r in (28) by

$$\langle r\rangle=\frac{\int dr\, r|A_1|^2}{\int dr|A_1|^2}\equiv\frac{\int dr\, r|C_1(r)|^2}{\int dr|C_1(r)|^2}. \tag{29}$$

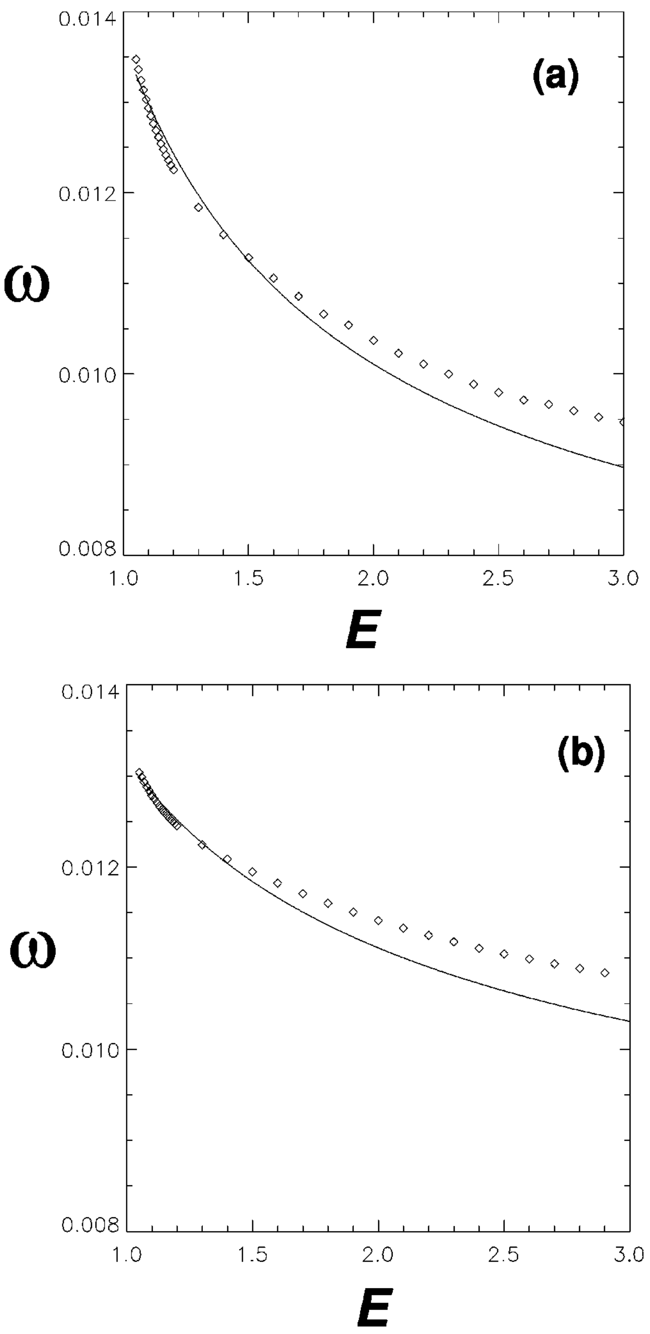

FIG. 13. Comparison of the frequency of rotation of trapped DW versus the input pump amplitude E between formulas (28) and (29) (solid lines) and numerical simulations (diamonds) for $m=1$ [panel (a)] and $m=2$ [panel (b)]. Parameters as in Fig. 11.

Figure 13 provides quantitative support for our prediction (28) with r replaced by $\langle r\rangle$ given in (29). The frequency of rotation has been evaluated from numerical simulations and plotted as a function of E for $m=1$ and $m=2$. The full lines in Fig. 13 are the analytical results of (28) and (29). The agreement with the angular frequency observed close to threshold, where we expect our analysis to be valid, is excellent in spite of the drastic approximations made, such as the form of the solution (27) in separable polar variables and the neglect of diffraction in (29).

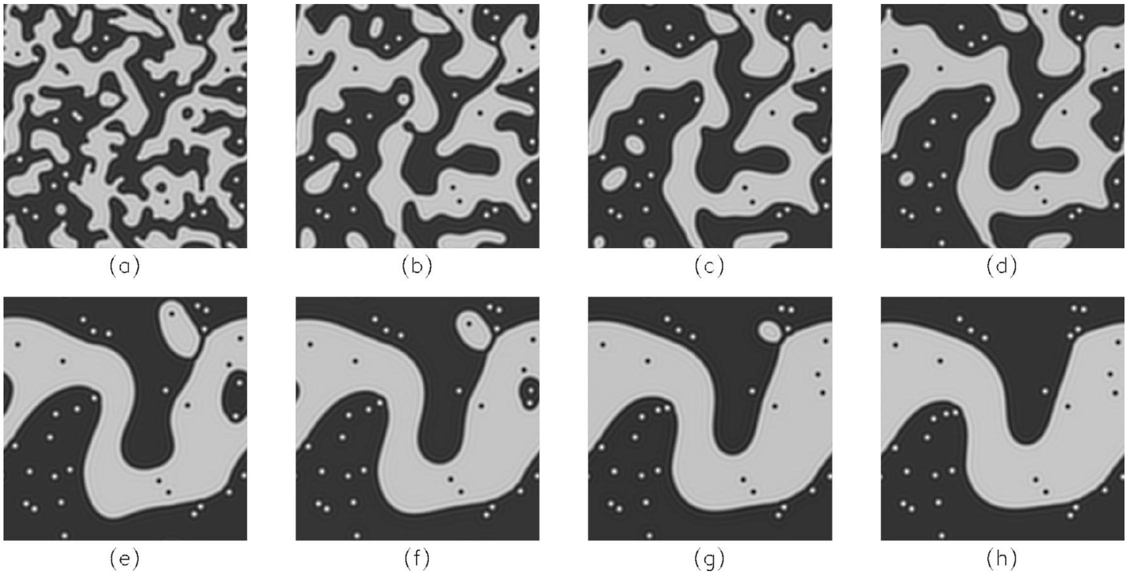

FIG. 14. Phase dynamics in the DRDOPO above the threshold for the formation of cavity solitons. The figures show Re(A_1) in the transverse plane at (a) $t=30$, (b) $t=90$, (c) $t=150$, (d) $t=210$, (e) $t=660$, (f) $t=900$, (g) $t=1140$, and (h) $t=1380$. $E=2.5$, transverse domain width 250 and other parameters as in Fig. 2.

V. CHARACTERIZATION AND STABILITY OF DARK-RING CAVITY SOLITONS IN DOPO

In Sec. III we pointed out that for sufficiently high values of the pump, shrinking domains in the DRDOPO, instead of collapsing to zero area, eventually form spatial solitary waves. An example of this is shown in Fig. 14, where an initial random arrangement of domains evolves towards a final state consisting of a distribution of solitary waves (or cavity ''solitons''). The images are obtained by integrating Eqs. (1) on a 256×256 grid with periodic boundary conditions using a split-step algorithm. The solitons consist of a peak in the signal intensity at the center, surrounded by a dark ring where the signal intensity is zero [Fig. 15(a)]. For that reason we term them dark ring cavity solitons (DRCS). This dark ring is what remains of the DW although the fields in the region bounded by the ring no longer correspond to a stationary homogeneous solution of the DRDOPO [Fig. 15(b)]. When considering a radial cut through the DRCS, one can again view the soliton as a homoclinic orbit which spirals out from one of the homogeneous fixed points in the complex signal plane and returns to the same fixed point asymptotically. The fact that DRCS are associated with homoclinic rather than heteroclinic orbits clearly shows that they are not circular domain walls [8]. Since there are two homoclinic orbits, each associated with a different homogeneous fixed point, there are obviously DRCS with two opposite phases: peaks with positive (negative) values of U surrounded by areas where U is negative (positive).

The oscillatory tails of the DW are a prerequisite for the formation of solitons: there is no counterpart to these structures in diffusive systems whose domain boundaries decay monotonically. Nevertheless, the presence of oscillations is not a sufficient condition. It is only when the amplitudes of these oscillations become large enough (on increasing the pump or decreasing Γ, for instance) that solitons appear. As an example, when $\Delta_1=0$ and $\Gamma=1$, solitons are observed in simulations only for $E\geqslant2.21$.

Another indication of this requirement is the absence of solitons in the SRDOPO. With diffraction of the pump field neglected, DW in the SDROPO have lower frequency, smaller amplitude spatial oscillations than those in the DRDOPO (cf. Fig. 2).

Simulations of Eqs. (1) can find stable solitons given appropriate initial conditions. In order to find all soliton solutions, stable and unstable, and thereby uncover the nature of the bifurcations from which these structures emerge, we analyze Eqs. (3) directly, with ∂_{xx} replaced by ∇^2. The solutions we seek are invariant with respect to rotations about their center and so $\boldsymbol{\nabla}^2$ can be written as

$$\boldsymbol{\nabla}^2=\frac{\partial^2}{\partial r^2}+\frac{1}{r}\frac{\partial}{\partial r}, \tag{30}$$

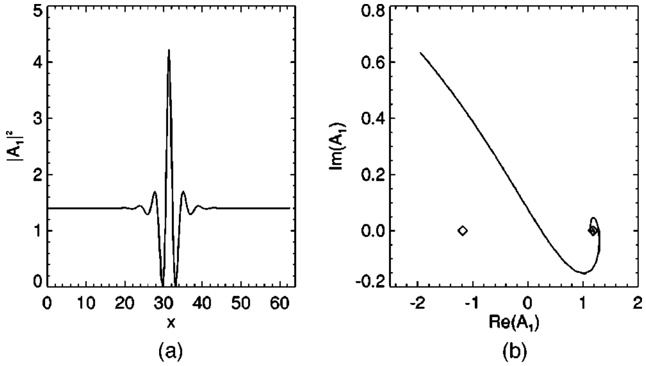

FIG. 15. (a) Plot of the signal intensity on a one-dimensional section through the center of a DRCS. (b) The soliton in (a) plotted in the complex A_1 plane. The diamonds indicate the stationary, homogeneous solutions. $E=2.4$, other parameters as in Fig. 2.

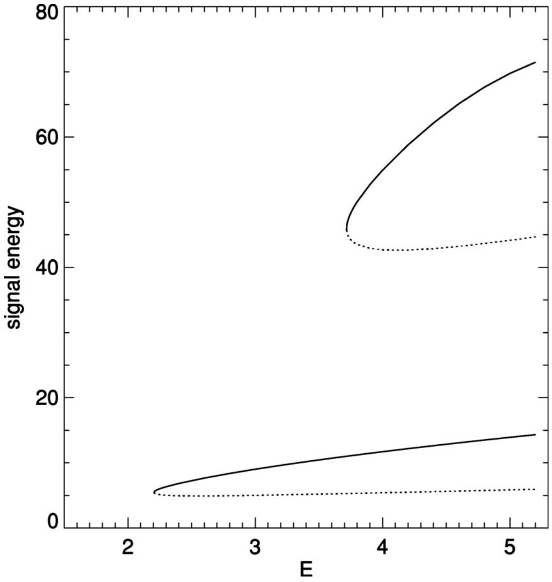

FIG. 16. Bifurcation diagram showing the existence of two types of cavity soliton solutions in the DRDOPO ($\Delta_1 = 0$, $a = 0.5$, $\Gamma_0 = 1$). Both types of solution emerge from saddle node bifurcations. Solid lines denote stable solutions, and dashed lines, unstable ones. The lower pair of branches corresponds to the DRCS.

where r is a radial coordinate relative to an origin at the center of the soliton.

Stationary solutions of Eqs. (3) which satisfy the boundary conditions

$$\partial_r A_0(r=0) = \partial_r A_1(r=0) = 0,$$
$$A_0(r\to\infty) = A_0^s, \tag{31}$$
$$A_1(r\to\infty) = A_1^s$$

can be found using the method referred to in Sec. II and described in detail in the Appendix. Their stability (at least to radially symmetric perturbations) can also be calculated simply by computing the spectrum of the Jacobian of the system around the soliton solution. This enables us to draw bifurcation diagrams such as Fig. 16 for $\Delta_1 = 0$ which shows the DRCS emerging from a saddle-node bifurcation at $E = 2.21$. The quantity plotted on the vertical axis of Fig. 16 and subsequent bifurcation diagrams is the soliton (signal) energy $\mathcal{E}$ defined as

$$\mathcal{E} = \int_0^\infty |A_1(r) - A_1(r\to\infty)|^2 r\, dr. \tag{32}$$

Also shown in Fig. 16 is another pair of solution branches corresponding to a different kind of spatial soliton. These solutions still have a dark ring around the central part but display a local dip of the signal intensity close to the center (a gray spot) unlike the previous family of DRCS (Fig. 17). Their spontaneous formation from collapsing circular domains has been observed in simulations of Eqs. (1) for $E > 3.72$, although the first family of DRCS is also stable in this region. It is important to stress that this second family of DRCS is also represented by homoclinic orbits in the complex phase space of the signal field [see Fig. 17(b)]. The central region has a different amplitude and phase with respect to the first family of DRCS but the homoclinic orbit still ends up far from any fixed point representing a homogeneous solution. The existence of yet more soliton solutions surrounded by a dark ring has not been ruled out. The coexistence of cavity solitons of different sizes is a novel result with potential applications in the design of optical memories. Lattices of the two cavity solitons can be superimposed to greatly increase the information storage of the DOPO used as a memory array. Applications of DOPO cavity solitons to information technology will be discussed elsewhere.

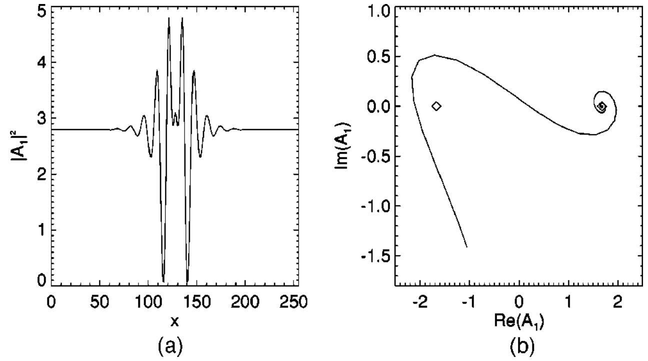

FIG. 17. (a) Plot of the signal intensity on a one-dimensional section through the center of a cavity soliton. The soliton belongs to the stable branch of the pair at the top right of Fig. 15. (b) The soliton in (a) plotted in the complex A_1 plane. The diamonds indicate the stationary, homogeneous solutions. $E = 3.8$, other parameters as in Fig. 2.

The DRCS do not exist only at resonance, which would make them difficult to observe, but also for $\Delta_1 > 0$, as Fig. 18(a) shows. As Δ_1 increases, however, the value of E at which the solitons appear also increases progressively following the signal generation threshold. The size of the DRCS also increases with the detuning. We are able to locate in the (E, Δ_1) plane the line of saddle-node bifurcations from which the DRCS emerge by using the method described in the Appendix. Figure 19 shows a drastic lowering

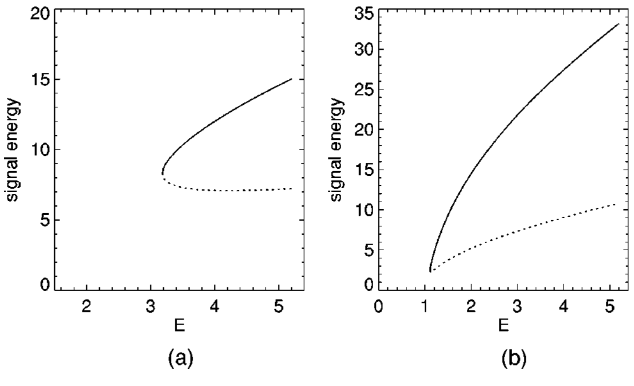

FIG. 18. Bifurcation diagrams showing the DRCS solution branches for (a) $\Delta_1 = 0.5$ (other parameters as in Fig. 14) and (b) $\Gamma_0 = 0.2$ (other parameters as in Fig. 14). Solid lines denote stable solutions, and dashed lines, unstable ones.

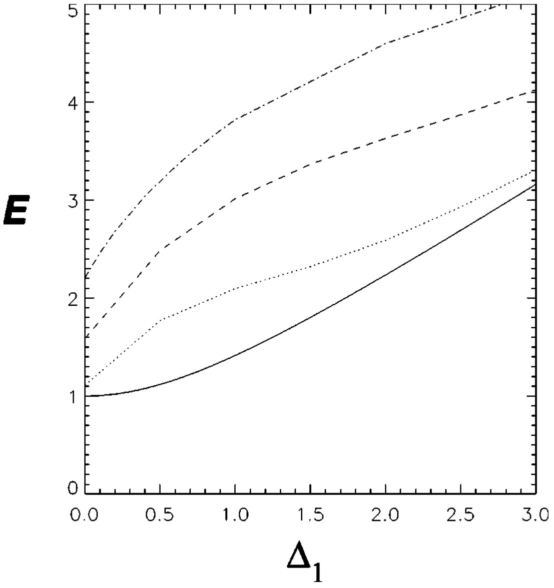

FIG. 19. Threshold for the appearance of cavity solitons in the (E,Δ_1) parameter space. The solid line is the signal threshold, the dotted line is the DRCS threshold for $\Gamma=0.2$, the dashed line for $\Gamma=0.6$ and dashed-dotted line for $\Gamma=1$.

of the threshold of DRCS for cavities of higher finesse for the pump field [27]. This is a very important fact with regard to possible experimental observation of DRCS in DOPO. The lowering of the DRCS threshold is in agreement with the diagrams of Fig. 4(a); large amplitude oscillations of the DW tails are intrinsically related to the pump diffraction and are the key element for the stabilization of DRCS.

Since DRCS in the DRDOPO exist for $\Delta_1 \geqslant 0$ they are unrelated to any modulational instability. They cannot therefore be interpreted as single peaks of a pattern, unlike the structures in Ref. [5]. One advantage of the DRCS over the usual cavity solitons due to the simultaneous presence of a pattern and a homogeneous solution is their broad range of existence. In the past, and in analogy with the one-dimensional case (Sec. II), similar spatial structures have been said to arise as the result of an interaction between two moving fronts, each of which separates a pair of homogeneous solutions [17]. As the fronts approach each other their oscillatory tails lock together and the fronts are pinned. This picture, however, cannot be generalized to two spatial dimensions where there is no real pairwise interaction of fronts but rather a single front interacting with itself and where local curvature effects of the fronts play such an important role. Nevertheless, it remains true that the spatial oscillations in the collapsing DW are a necessary feature for the formation of the cavity solitons. Their importance seems to lie in generating, through an interference effect, a local ''hotspot'' (or ''hot-circle'' in the case of the second family of DRCS described above) of the appropriate intensity and phase in the interior of the collapsing DW. This is not possible if the spatial oscillations are too small in amplitude, hence the existence of a threshold for DRCS formation.

It is interesting to look at the local energy balance within DRCS. Consider the total energy $\mathcal{S}$ at any point

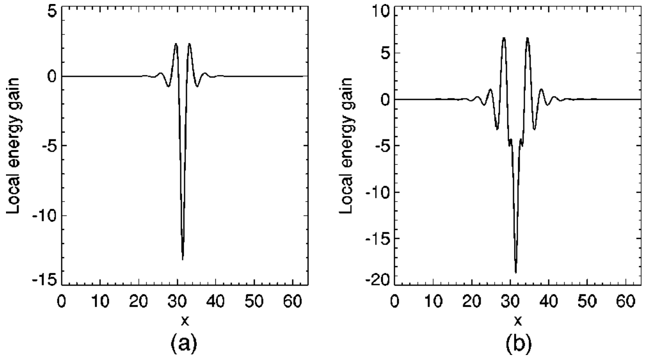

FIG. 20. The local energy gain [left-hand side of Eq. (34)] on a transverse slice through two cavity solitons: (a) the DRCS of Fig. 15 and (b) the cavity soliton of Fig. 17.

$$\mathcal{S}=|A_0|^2+\Gamma|A_1|^2. \tag{33}$$

The factor of Γ arises from the normalizations of A_0 and A_1 [1]. Using Eqs. (1) it is easy to show that in steady state, when $\partial_t \mathcal{S}=0$,

$$\begin{aligned} -2\Gamma(|A_0|^2+|A_1|^2)+\Gamma E(A_0+A_0^*) &= -i\frac{a}{2}(A_0^*\nabla^2 A_0-A_0\nabla^2 A_0^*) \\ &\quad -ia\Gamma(A_1^*\nabla^2 A_1-A_1\nabla^2 A_1^*). \end{aligned} \tag{34}$$

The first term on the left-hand side represents losses through the cavity mirrors. The second term is the energy put into the system by the external pump. The nonlinear terms merely transfer energy from one field to the other with no loss or gain and so they make no contribution to Eq. (34). The two terms on the right-hand side represent transverse energy transport caused by diffraction. The solution is formed when the excess of the left-hand side of Eq. (34), due to the deviation from the homogeneous steady state, is counterbalanced by diffraction.

In Fig. 20 we plot the left-hand side of Eq. (34) across a slice through a DRCS of each family. It can be seen that at the center, the net contribution of the damping and driving terms is negative and the energy deficit must be compensated by a transverse transport of energy towards the center. Conversely, the sum of the driving and damping terms in the region of the dark ring is positive which implies a transport of energy out of the dark ring. The picture that emerges, then, is of energy moving from the dark ring to the bright peak (or area) at the center to sustain the DRCS.

Finally, we mention that in the nondegenerate case when the frequencies of the signal, A_1, and idler, A_2, fields are well separated, the symmetry $A_1 \to -A_1$ of the degenerate case is replaced by the symmetry $[A_1,A_2^*] \to e^{i\phi}[A_1,A_2^*]$. The pair of homogeneous stationary states of the degenerate case is replaced by an entire family of possible homogeneous stationary solutions with arbitrary phase. The main effect of this nondegenerate symmetry is to destabilize some of the Ising-type DW and DRCS described in this paper via a progressive shift of the phase, since the real and imaginary parts of the signal field are not constrained to be equal to zero simultaneously.

VI. DISCUSSION AND CONCLUSIONS

The nature, characteristics, stability, interaction, and evolution of diffractive domain walls and dark ring cavity solitons in degenerate OPO have been exhaustively analyzed. Our study builds on previous short studies that focused on one or a few of these topics [3–5,8]. In particular, we have shown that DW of the Ising type are commonplace in the signal field of degenerate OPO in both the singly and doubly resonant configurations.

The DW in DOPO often correspond to spiral heteroclinic connections and present oscillatory tails. Thresholds separating oscillatory from nonoscillatory tails have been identified in both the singly and doubly resonant cases. This analysis allows us to exclude dark ring spatial solitons, which require large amplitude oscillations in the tails of the DW, from large regions of the parameter space. It is important to note however that such soliton structures in 2D do not correspond to circular domain walls [8] since they are homoclinic solutions which end very far from the homogeneous fixed point present in a DW.

DW in DOPO may appear to be elusive to experimental observation since they either appear during transients or else quickly move across and out of the optical beam in the presence of walk-off [24]. We have discussed a simple experimental arrangement based on an input pump beam of doughnut shape and unit topological charge (corresponding to Gauss-Laguerre modes of zero radial index and azimuthal index of one) for the indefinite trapping of single and multiple DW. These structures rotate in the transverse plane due to diffraction. Such a rotation can be overcome by fast detection systems which can identify sudden periodic disappearances of the signal intensity at certain distances from the optical axis, thereby providing evidence for the existence of a DW. We are currently investigating the possibility of utilizing these rotating structures containing DW for the manipulation of trapped cold atoms.

After this paper was completed, Ref. [28] appeared. In Ref. [28] it is shown that the stability of localized structures in DOPO is enhanced by pump diffraction. We note that this fact was already stated in Ref. [4], that their Eqs. (7) and (8) have already appeared and have been discussed in Ref. [4] and that in a confocal resonator every ray does not have the same optical length in one cavity trip thus invalidating their usage of Eqs. (1) with changing diffraction coefficients.

ACKNOWLEDGMENTS

We are indebted to G. Harkness for useful discussions. We acknowledge support from EPSRC (Grants Nos. GR/M 19727 and GR/M 31880), SHEFC (Grant VIDEOS), and the European Commission (TMR Network QSTRUCT, Contract No. FMRXCT960077). G.L.O. acknowledges support from SGI.

APPENDIX

In this Appendix we describe the relaxation method [29,30] used to compute stationary DW and soliton solutions of the DOPO equations as well as the technique for calculating their stability. Consider Eqs. (3) for stationary solutions of the doubly resonant DOPO in one transverse dimension. To solve these equations on a grid of N points we define the variables $\{A_0^{(i)}\}$ and $\{A_1^{(i)}\}$, $i=1\ldots N$, the fields at the grid points. We then have the following set of simultaneous equations to solve

$$\begin{aligned}&\nabla_d^2 A_0^{(i)} - 2i\left(\frac{\Gamma}{a}\right)[-A_0^{(i)} + E - (A_1^{(i)})^2] = 0,\\ &\nabla_d^2 A_1^{(i)} - i\left(\frac{1}{a}\right)[-A_1^{(i)} - i\Delta_1 A_1^{(i)} + A_0^{(i)}(A_1^{(i)})^*] = 0,\end{aligned} \tag{A1}$$

where ∇_d^2 is a discretized version of the Laplacian in one dimension. We choose to calculate the $\nabla_d^2 A_0^{(i)}$ and $\nabla_d^2 A_1^{(i)}$ terms using fast Fourier transforms (FFTs) [30] rather than a more common finite difference approximation. The former has the advantage of greater accuracy $[O(dx^N)]$ so that in principle a larger space step can be used. Thus we take the FFT of the field made up of the $\{A_0^{(i)}\}$ or $\{A_1^{(i)}\}$, multiply by $(-k^{(i)})^2$, where $\{k^{(i)}\}$ is an array of spatial frequencies, and take the inverse transform. We then have two arrays containing the values of $\nabla_d^2 A_0^{(i)}$ and $\nabla_d^2 A_1^{(i)}$ at each point on the grid, from which the value to be used in each of the equations (A1) can be read. The FFT imposes the constraint of periodic boundary conditions but in practice this is not too much of a problem: in one dimension it simply means that we can only look at even numbers of DW.

To arrive at a solution of equations (A1) we start from an initial guess for the $\{A_0^{(i)}\}$ and $\{A_1^{(i)}\}$ and apply a multidimensional Newton's method [30]. At each iteration of the method we compute the magnitude of the left hand side of Eqs. (A1), which should be zero for an exact solution. The process is continued until this quantity falls below some predetermined tolerance, whereupon we have our solution.

Once a solution has been calculated its stability can also be determined. We compute the Jacobian matrix of Eqs. (1) numerically around the known solution. Then it is just a matter of calculating the eigenvalues and eigenvectors of the Jacobian. At least one eigenvalue with positive real part implies instability of the solution. Otherwise it is stable.

A modification of the method to deal with radially symmetric solutions in two dimensions is quite straightforward. The Laplacian is now given by Eq. (30). The $\partial/\partial r$ and $\partial^2/\partial r^2$ terms are again evaluated in Fourier space using FFTs, and the results combined to give ∇_d^2. In order to satisfy the periodic boundary conditions which the discrete Fourier transform requires, we embed our grid of N points in a larger grid of $2N$ points by reflecting our solution about the point $r=0$. While the smaller grid contains the fields from $r=0$ to $r=r_{\max}$, the larger grid contains (formally) the fields from $r=-r_{\max}$ to $r=r_{\max}$. The derivatives are then evaluated on the larger grid where periodic boundary conditions are certainly satisfied. Note that the grid of $2N$ points is only used to evaluate the spatial derivative terms; the search for a solution using the Newton method is still carried out on the smaller grid of N points, both for reasons of efficiency and to avoid spurious, asymmetric solutions which might be generated on the larger grid.

The stability of a solution is computed in the same way as it is in one dimension: the Jacobian of the solution is calculated and its eigenvalues and eigenvectors found numerically. Of course, this simple technique, which omits any azimuthal dependence, can only check for stability with respect to radially symmetric perturbations.

[1] G.-L. Oppo, M. Brambilla, and L.A. Lugiato, Phys. Rev. A **49**, 2028 (1994); G.-L. Oppo, M. Brambilla, D. Camesasca, A. Gatti, and L.A. Lugiato, J. Mod. Opt. **41**, 1151 (1994); M. Brambilla, D. Camesasca, S. Sinclair, and G.-L. Oppo (unpublished).

[2] G.J. de Valcarcel, K. Staliunas, E. Roldan, and V.J. Sanchez-Morcillo, Phys. Rev. A **54**, 1609 (1996).

[3] S. Trillo, M. Haelterman, and A. Sheppard, Opt. Lett. **22**, 970 (1997).

[4] G.-L. Oppo, A. J. Scroggie, and W. J. Firth, Technical Digest IQEC '98, 172, 1998; Technical Digest EQEC '98, 245, 1998; G.-L. Oppo, A.J. Scroggie, and W.J. Firth, J. Opt. B: Quantum Semiclassical Opt. **1**, 133 (1999).

[5] K. Staliunas and V.J. Sanchez-Morcillo, Opt. Commun. **139**, 306 (1997); Phys. Rev. A **57**, 1454 (1998).

[6] S. Trillo, and M. Haelterman, Opt. Lett. **23**, 1514 (1998).

[7] D.V. Skryabin and W.J. Firth, Opt. Lett. **24**, 1056 (1999); D.V. Skryabin, Phys. Rev. E **60**, R3508 (1999).

[8] M. Le Berre, D. Leduc, E. Ressayre, and A. Tallet, J. Opt. B: Quantum Semiclassical Opt. **1**, 153 (1999); M. Tlidi, M. Le Berre, A. Ressayre, A. Tallet, and L. Di Menza, Phys. Rev. A **61**, 043806 (2000).

[9] Special issue on optical parametric devices and processes [J. Opt. Soc. Am. B **16** (1999)].

[10] M. Vaupel, A. Maître, and C. Fabre, Phys. Rev. Lett. **83**, 5278 (1999).

[11] S. Longhi, J. Mod. Opt. **43**, 1089 (1996).

[12] P. Coullet, J. Lega, B. Houchmanzadeh, and J. Lajzerowicz, Phys. Rev. Lett. **65**, 1352 (1990).

[13] S. Ciliberto, P. Coullet, J. Lega, E. Pampaloni, and C. Perez–Garcia, Phys. Rev. Lett. **65**, 2370 (1990).

[14] K. Ouchi and H. Fujisaka, Phys. Rev. E **54**, R3895 (1996).

[15] R.H. Hardin and F.D. Tappert, SIAM Rev. **15**, 423 (1973).

[16] K. Kawasaki and T. Ohta, Physica A **116**, 573 (1982).

[17] P. Coullet, C. Elphick, and D. Repaux, Phys. Rev. Lett. **58**, 431 (1987).

[18] It has recently been found that in the parametrically driven damped nonlinear Schrödinger equation stable configurations of several solitons with no oscillating tails can be found [see I.V. Barashenkov and E.V. Zemlyanaya, Phys. Rev. Lett. **83**, 2568 (1999)]. The equations studied there correspond to the SRDOPO case with a purely imaginary (instead of a purely real) coefficient of the nonlinearity and the analysis dealt with solitons with tails decaying to zero. Despite these differences, we cannot exclude that similar behavior, although unlikely, may also take place in our DOPO equations.

[19] A.J. Bray, Adv. Phys. **43**, 357 (1994); see also J.D. Gunton, M. San Miguel, and P. Sahni, in *Phase Transitions and Critical Phenomena*, edited by C. Domb and J. Lebowitz (Academic, London, 1983), Vol. 8, pp. 269–466.

[20] S.M. Allen and J.W. Cahn, Acta Metall. **27**, 1085 (1979).

[21] R. Gallego, M. San Miguel, and R. Toral, Phys. Rev. E **61**, 2241 (2000).

[22] The scaling behavior of the structure factor shown in Ref. [14] corresponds to $\Delta_1 < 0$ in Eq. (19). For negative detunings there exist stable spatially modulated solutions in addition to the homogeneous solutions. The existence of these solutions, however, should have no bearing on the scaling behavior of the homogeneous domains.

[23] Note, however, that when $\Gamma = 1$ there exists a time-dependent Lagrangian for the DOPO equations.

[24] M. Santagiustina, P. Colet, M. San Miguel, and D. Walgraef, Opt. Lett. **23**, 1167 (1998).

[25] M. Abramowitz and I. Stegun, *Handbook of Mathematical Functions* (Dover, New York, 1972); K. Dholakia, N.B. Simpson, M.J. Padjett, and L. Allen, Phys. Rev. A **54**, R3742 (1996).

[26] W.J. Firth and A.J. Scroggie, Phys. Rev. Lett. **76**, 1623 (1996).

[27] G.-L. Oppo, A.J. Scroggie, S. Sinclair, and M. Brambilla, J. Mod. Opt. **47**, 2005 (2000).

[28] V.J. Sanchez-Morcillo and K. Staliunas, Phys. Rev. E **61**, 7076 (2000).

[29] W.J. Firth and G.K. Harkness, Asian J. Phys. **7**, 665 (1998).

[30] W.H. Press, B.P. Flannery, S.A. Teukolsky and W.T. Vetterling, *Numerical Recipes* (Cambridge University Press, Cambridge, 1986).